Check for updates

Received: 21 December 2023 | Revised: 15 March 2024 | Accepted: 31 March 2024

DOI: 10.1002/app.55546

RESEARCH ARTICLE

Applied Polymer Science WILEY

Multiscale mechanics of polydimethylsiloxane: A comparison of meso- and micro-cyclic deformation behavior

Lihua Lou[1] | Nicole Bacca[1] | Marshall S. Ma[2,3] | Pranjal Nautiyal[1] | Thomas G. Bifano[2,3] | Arvind Agarwal[1]

[1]Plasma Forming Laboratory, Mechanical and Materials Engineering, College of Engineering and Computing, Florida International University, Miami, Florida, USA

[2]Mechanical Engineering, Boston University, Boston, Massachusetts, USA

[3]Photonics Center, Boston University, Boston, Massachusetts, USA

Correspondence
Lihua Lou, Plasma Forming Laboratory, Mechanical and Materials Engineering, College of Engineering and Computing, Florida International University, Miami, FL 33174, USA.
Email: llou@fiu.edu

Funding information
National Science Foundation, Grant/Award Number: EEC-1647837; Florida Heart Foundation

Abstract

Despite plenty of static and dynamic mechanical measurements and modeling for bulk polydimethylsiloxane (PDMS) specimens, a notable gap exists in comprehensively understanding the dynamic mechanics under large cycle, low strain conditions, especially for microscale samples. This study integrates tensile testing and nanoindentation techniques to compare dynamic mechanical response for bulk PDMS samples and μ-pillars. The results from cyclic tensile testing, which involved up to 10,000 cycles at a strain range of 10%–20%, indicate a stabilization of energy dissipation rate after the initial 25 cycles. This attributes to stress relaxation and strain hardening, validating by rapid dual-phase exponential decay in maximum stress, coupled with an incremental increase in elastic modulus. In comparison to tensile testing, μ-pillars exhibited a 0.82% reduction in stiffness, stabilizing ∼600th cycle. Concurrently, there was an approximately twofold increase in approaching distance during the initial 120 cycles, and an approximately fourfold increase in dissipated energy over the first 80 cycles, before reaching a plateau. This lagging hysteresis effect attributes to the distribution of the resultant force, including top tension, bottom compression, and base tilt. Overall, this study illuminates temporal mechanical deformations in PDMS under two application scenarios, enhancing our understanding of PDMS mechanical behavior.

KEYWORDS

biomaterials, mechanical properties, molding

1 | INTRODUCTION

Polydimethylsiloxane (PDMS),[1,2] consisting of repeating units of —$Si(CH_3)_2O$—, is an advanced organosilicon macromolecule polymer distinguished by its mobile carbon-silicone linkages. Owing to excellent dielectric isolation property, it was initially employed for encapsulating electronic components[3] in the early 1980s. Due to its facile fabrication, high flexibility, chemical neutrality, excellent biocompatibility, optical transparency, and resistance to liquid penetration,[4] it is gradual increase in the popularity within micro- and nano-technologies,[2] for example, microfluidic devices, sensors, and optical systems in the late 1990s and early 2000s. In particular, it retains thermal stability across temperatures ranging from −50 to +200°C, demonstrating strong resistance to water,

 © 2024 Wiley Periodicals LLC.

oxygen, ozone, and ultraviolet light, while naturally repelling water. Regarding its mechanical properties, its Young's modulus can be adjusted based on the concentration of the crosslinker. PDMS's adoption in microfluidic devices[2] was particularly significant, as it allowed for the creation of complex, miniaturized systems. This period marked a turning point in the utilization of PDMS in advanced technological applications, significantly impacting fields, especially biomedical engineering.[5] In the realm of cardiac engineering, PDMS devices have been employed in the design of heart-on-a-chip platforms,[6] the fabrication of cardiac tissue scaffolds, and the development of microfluidic devices[7] for cardiac cell culture. Additionally, they have been utilized in the creation of implantable sensors,[8] the manufacturing of vascular grafts,[9] and the formulation of drug delivery systems.[10]

Within the spectrum of its applications in cardiac engineering, the use of PDMS μ-pillars[11–14] stands out as a novel approach. These pillars function as mechanical sensors,[12,14] designed to detect and quantify the contractile forces exerted by cardiomyocytes or cardiac tissues. When these forces are applied, the pillars undergo bending or deformation. The extent of this deformation can be quantified to calculate the applied forces, utilizing high-resolution imaging techniques. The data derived from these measured contractile forces hold significant implications for research areas such as drug testing and the maturation of cells and tissues. Nonetheless, considering the beating rate of cardiomyocytes or cardiac tissues, which ranges from 30 to 100 beats per minute (bpm),[11,13,15] there are concerns regarding the long-term mechanical stability of PDMS μ-pillars and the reliability of using their stiffness to accurately calculate contractile forces.

The static and dynamic mechanical properties of bulk PDMS samples have been widely studied compared to μ-pillars. In the context of static mechanics, Seo et al.[4] have investigated the impact of curing agent concentration on the stiffness of PDMS substrates (Sylgard 184). This was achieved through various testing methods, including bulk tensile testing, macroscale compression testing, and nanoscale atomic force microscopy (AFM) nanoindentation testing. Their findings indicate that the elastic modulus of PDMS substrates reaches its maximum at a base to curing agent ratio of 10:1, compared to other tested ratios such as 10:0.25, 10:0.5, 10:2, and 10:4. Similarly, test was conducted by Wang et al.[15] using a compression test, their results elucidated a linear relationship between the elastic modulus of PDMS and the quantity of the curing agent used. Additionally, they observed that the relationship between the elastic modulus and the ratio of base to curing agent (5:1, 7:1, 10:1, 16.7:1, 25:1, and 33:1) follows an exponential decay pattern.

In the study of dynamic mechanical behaviors of PDMS, tensile, compression, and dynamic mechanical analysis (DMA) methods are commonly used. Lee et al.[16] researched the effects of cyclic compression and varying base-to-curing agent ratios (5:1, 10:1, and 15:1) on the mechanical stability of PDMS. Their experiment involved subjecting PDMS to 0%–20% strain over 100 cycles. They observed a hysteresis loop, with the 10:1 base-to-curing agent ratio exhibiting the highest mechanical damping, as indicated by the greatest energy dissipation. Additionally, viscoelastic properties were noted, manifesting as strain hardening behaviors. This was characterized by increased elastic modulus and peak stress concurrent with the rising number of cycles across all base-to-curing agent ratios. The researchers attributed this strain hardening to alterations in the pendant chains of the PDMS structure. Babu and Gundiah[17] conducted a study focusing on the influence of various base-to-curing agent ratios on the dynamic mechanical properties of PDMS across a frequency range of 0.5–100 Hz. Their findings revealed that as the degree of crosslinking increases, the complex modulus of PDMS experiences a significant reduction. Specifically, the complex modulus decreases by a factor of five times more in lightly crosslinked samples (with a 5:1 ratio) than those highly crosslinked (with a 10:1 ratio). Song et al.[18] studied the dynamic behaviors of PDMS films using cyclic tensile test, where 20 tests within strain range of 30%–130% is applied.

Despite existing research, there remains a gap in understanding the large cycle, low strain dynamic mechanical properties of bulk PDMS in tensile samples and μ-pillars. To address this, we conducted studies on commonly used PDMS with a base-to-curing agent ratio of 10:1. For bulk PDMS dog-bone tensile samples, we measured their response to 10,000 cycles with a strain range of 10%–20%. For μ-pillars, we conducted 1000 cycles of nanoindentation testing while they were in a suspended state to assess their mechanical robustness under dynamic conditions. The primary objective of this study is to investigate and compare the viscoelastic behaviors and underlying mechanisms in both bulk and micro-scale testing contexts.

2 | EXPERIMENTAL

2.1 | Materials

The SYLGARD™ 184 silicone elastomer kit, including a base and a curing agent, was purchased from Dow

10974628, 0, Downloaded from https://onlinelibrary.wiley.com/doi/10.1002/app.55546 by Florida International University, Wiley Online Library on [19/04/2024]. See the Terms and Conditions (https://onlinelibrary.wiley.com/terms-and-conditions) on Wiley Online Library for rules of use; OA articles are governed by the applicable Creative Commons License

Chemical Company (Fort Lauderdale, FL). The ASTM D-638 Type V specimen die was purchased from Pioneer-Dietecs Corporation (Weymouth, MA).

2.2 | PDMS sample preparation

PDMS specimens were synthesized by homogeneously blending the elastomer base with the curing agent in mass ratios of 10:1. Once mixed, the solution was poured into a 90 mm diameter glass petri dish. Following this, the mixture was subjected to a degassing process in a vacuum desiccator for 25 min to eliminate entrapped air bubbles. This was followed by a curing phase within a laboratory oven set at 100°C, sustained for a duration of 35 min. Dog-bone shaped specimens with dimensions of 3.5 mm in thickness, 3.6 mm in width, and a gauge length of 14 mm, were cut using the ASTM D-638 Type V die.

In parallel, PDMS μ-pillar with a weight of ~700 mg, characterized by a rectangular base and a semi-spherical cap, were synthesized using the methodology detailed by Javor et al.[19] Briefly, μ-pillar were fabricated utilizing the replica molding technique. The curing process for these pillars was identical to that employed for the PDMS specimens, with the use of a polypropylene mold. After curing, the assembly was submerged in ethanol, enhancing detachment. The resultant μ-pillar dimensions are total height of 1460 μm, base length of 430 μm, base width of 390 μm, base height of 1280 μm, and semi-spherical cap diameter of 390 μm.

2.3 | Tensile testing

Mechanical properties of dog-bone samples were tested using Electroforce 2100 tensile tester manufactured by T.A. Instruments (New Castle, DE), as shown in Figure 1a. A sinusoidal waveform (Figure 1a) was applied for cyclic fatigue testing with minimum and maximum strains of 10% and 20%, respectively. Cyclic parameters were a frequency of 2 Hz and varied cyclic numbers of 25, 50, 75, 100, 250, 500, 750, 1000, 2500, 5000, 7500, and 10,000. Stress–strain curves were plotted to investigate the mechanical response of PDMS samples under a uniaxial external force. Elastic modulus (E, MPa) was measured as the slope of stress–strain curves at the initial section (Equation 1):[20]

$$E = \sigma/\varepsilon, \quad (1)$$

where σ and ε are stress (MPa) and strain (%), respectively.

2.4 | In-situ indentation

Mechanical properties of μ-pillar were testing using a Biosoft system from Bruker (Billerica, MA). For the cyclic

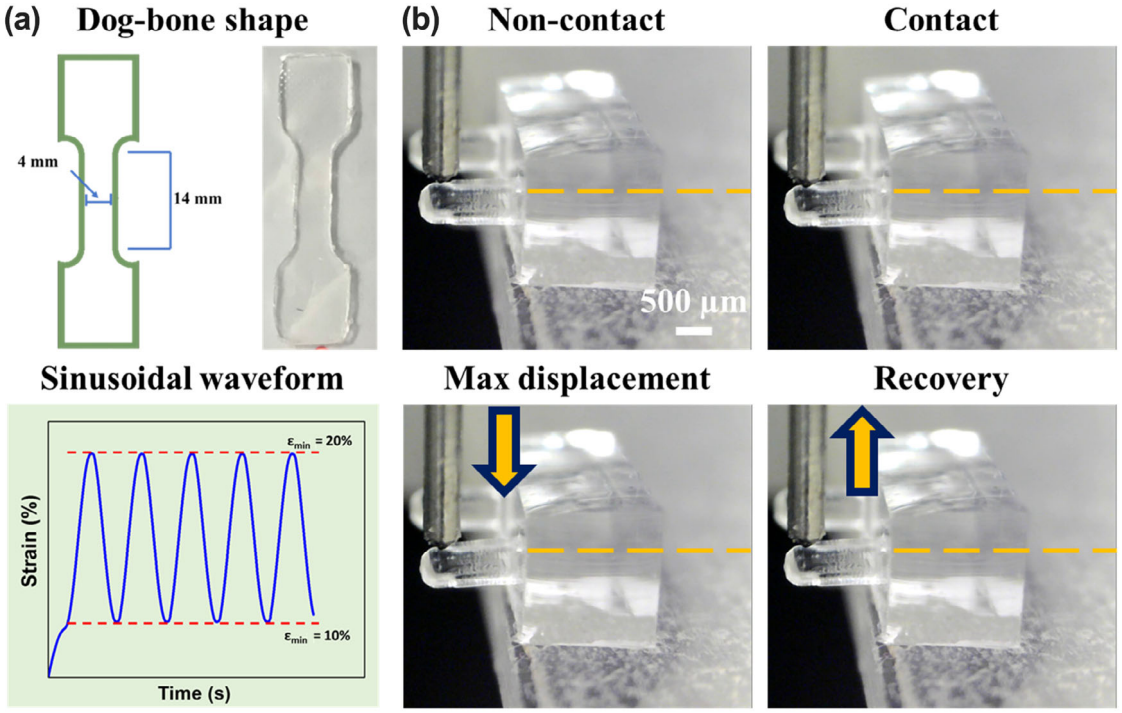

FIGURE 1 Sample and experiment setup. (a) Dog-bone shape tensile samples and sinusoidal waveform cyclic fatigue testing schedule. (b) Status of indentation process (initial contact, loading, and unloading). [Color figure can be viewed at wileyonlinelibrary.com]

10974628, 0, Downloaded from https://onlinelibrary.wiley.com/doi/10.1002/app.55546 by Florida International University, Wiley Online Library on [19/04/2024]. See the Terms and Conditions (https://onlinelibrary.wiley.com/terms-and-conditions) on Wiley Online Library for rules of use; OA articles are governed by the applicable Creative Commons License

indentation tests, a conospherical probe with a diameter of 400 μm was utilized, as illustrated in Figure 1b. The testing protocol involved displacement-controlled indentation combined with initial contact detection, conducting at a frequency of 0.05 Hz. The testing methodology included the following segments: approaching, loading and unloading at ±10 μm/s for ±100 μm, as depicted in Figure 1b. The probe was retracted at a controlled velocity of −10 μm/s for 15 s to ensure the complete detachment of the probe subsequent to the completion of the loading–unloading cycle. The indentation process was recorded by a real-time imaging endoscope to capture the probe-pillar contact and indentation position. The Oliver & Pharr model was used to analyze the stiffness of μ-pillar, where stiffness (S, N/m) was calculated based on Equation 2[21,22]:

$$S = \frac{\Delta F}{\Delta h}, \tag{2}$$

where ΔF and Δh represent absolute load and displacement change, respectively.

2.5 | Microstructural characteristics

The microstructural features of PDMS tensile specimens and micro-pillars, before and after cyclic loading and subsequently coated with a 5 nm gold layer, were captured and analyzed using a Schottky JEOL-F100 field emission scanning electron microscope (FESEM) manufactured by JEOL Ltd. (Tokyo, Japan). The imaging was performed at an acceleration voltage of 1 kV.

3 | RESULTS AND DISCUSSION

3.1 | Cyclic tensile testing

Uniaxial cyclic tensile stress–strain curves for PDMS dog-bone samples, subjected to a strain range of [10%, 20%] under sinusoidal loading, are graphically represented in Figure 2. As shown in Figure 2a–c, the acquired stress–strain curve is characterized by a non-terminating half-elliptical profile with two distinct phases. In Phase I, there is a gradual increase in stress corresponding to an increase in strain from 10% to 20%. Conversely, Phase II is marked by a gradual decrement in stress with a reduction in strain from 20% to 10%. The enclosed region by Phases I and II is hysteresis loop, indicating of energy dissipation. The energy dissipation is due to internal friction happening when wrinkle chains align, disentangle, or rectangle under external stress. This process includes stretching and reorientation of the silicone-oxygen backbone and the associated pendant methyl groups. This energy dissipation characteristics indicate of viscoelastic nature of the cross-linked PDMS network, paralleling findings by Lee et al.[16] Their research highlights the direct impact of the curing agent concentration on PDMS viscoelastic properties using cyclic compression testing, where the 1st and 100th cycle dissipated energy was calculated and analyzed.

In our approach, we analyzed the dynamic variation in energy dissipation across 10,000 tensile testing cycles. As shown in Figure 2, there is a notable decrease in energy dissipation correlating with increment of tensile cycle. To quantify the dynamic energy dissipation rate, we defined Equation 3:

$$\text{Energy dissipation rate}\,(\%) = \frac{{E_{\text{strain}}}^{a}}{{E_{\text{strain}}}^{1}} \times 100\%, \tag{3}$$

where $a > 1$, a is cycle number. As shown in Figure 2a, the observed energy dissipation rate is 11.10% at 25th cycle, 10.83% at 50th cycle, 10.37% at 75th cycle, and 10.28% at 100th cycle. Figure 2b demonstrates $a \sim 9.85\%$ energy dissipation rate across cycles ranging from 250 to 1000. Similarly, Figure 2c indicates $a \sim 9.99\%$ energy dissipation rate at 2500–10,000th cycles. The energy dissipation rate lower than 100% suggests PDMS dissipates less energy in the specific cycle than in the first cycle. Another notable observation is the stabilization of the energy dissipation rate at ~10% after the initial 25 cycles. These observed phenomena are potentially attributed to reduction in internal friction, and the phenomenon of stress relaxation and strain hardening. The reduction in internal friction is hypothesized to arise from the progressive linear alignment of polymer chains. Stress relaxation indicates PDMS adapts to the applied stress with microstructure stabilization, leading to a reduction in the internal forces. Strain hardening is characterized by an increased rigidity and reduced deformability of PDMS with the increase of cycle, consequently leading to a lower energy lost through internal friction and deformation processes.

To validate the hypothesis related to stress relaxation, we quantified the maximum stress and cycle relationship. As illustrated in Figure 3a, the reduction in maximum stress as of the initial cycle exhibited two distinct phases: an initial rapid reduction in stress during the initial 25 cycles followed by a plateau phase over 25–10,000th tensile cycles. In Figure 3b, the initial 25-cycle rapid stress reduction followed a dual-phase exponential decay pattern (Equation 4).[23,24]

$$\text{Max. stress} = A_1 e^{-B_1 t} + A_2 e^{-B_2 t} + C, \tag{4}$$

where A_1 and A_2 are initial stress levels of each decay phase, B_1 and B_2 are the decay constants for each phase, t is cycle number, and C is the asymptotic stress value the

10974628, 0, Downloaded from https://onlinelibrary.wiley.com/doi/10.1002/app.55546 by Florida International University, Wiley Online Library on [19/04/2024]. See the Terms and Conditions (https://onlinelibrary.wiley.com/terms-and-conditions) on Wiley Online Library for rules of use; OA articles are governed by the applicable Creative Commons License

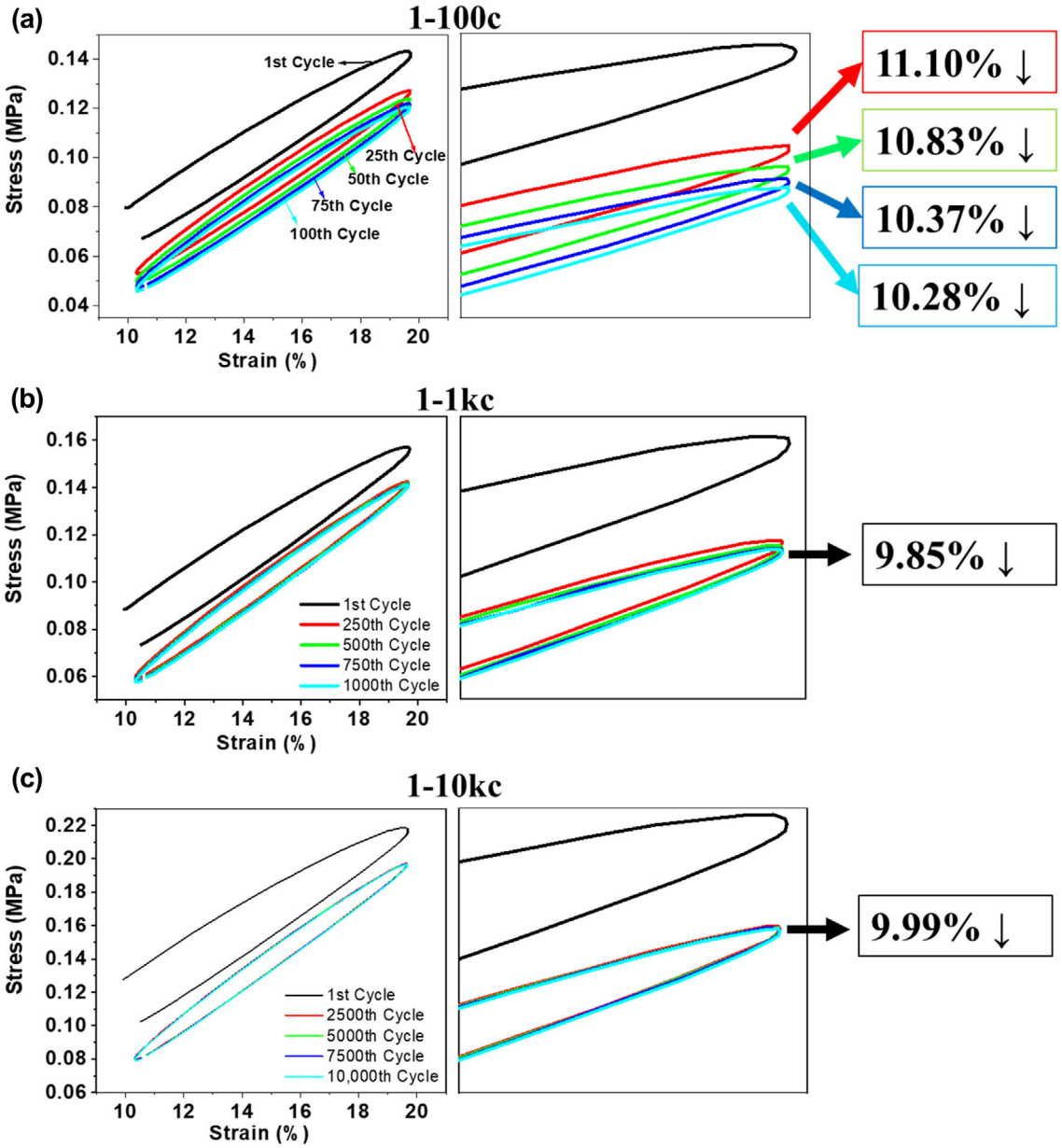

FIGURE 2 Cyclic tensile stress–strain curves, elastic strain energy, and maximum stress ($n = 3$). (a) Tensile strain–stress curves of dog-bone PDMS (polydimethylsiloxane) tensile samples after the 1st, 25th, 50th, 75th, and 100th testing cycles and the corresponding decrease in elastic strain energy. (b) Tensile strain–stress curves of dog-bone PDMS tensile samples after 1st, 250th, 500th, 750th, and 1000th testing cycles and corresponding decreasing in elastic strain energy. (c) Tensile strain–stress curves of dog-bone PDMS tensile samples after 1st, 2500th, 5000th, 7500th, and 10,000th testing cycles and corresponding decreasing in elastic strain energy. c, cycles; kc, 1000 cycles. [Color figure can be viewed at wileyonlinelibrary.com]

curve approaches as cycles increase. B_1 of 10.75 represents rapid chain alignment or entanglement disentangling. B_2 of 0.4 represents long-term structural rearrangement. The observed patterns in these two curves substantiate the presence of stress relaxation phenomena. It stems from the initial viscous behavior of PDMS, characterized by a relatively high stress response. Subsequently, PDMS starts to exhibit more elastic behavior, leading to stress reduction.

Similarly, to validate the hypothesis related to strain hardening, we quantitatively analyzed the elastic modulus and cycle relationship. Contrary to max stress behavior, elastic modulus, as depicted in Figure 3c, exhibited incremental increases of ~2.75%, 14.78%, and 61.84% at cycle intervals of 25–100th, 250–1000th, and 2500–10,000th, respectively, when compared to the modulus at the 1st cycle. In a detailed analysis of the elastic modulus across varying cycle intervals, distinct patterns of change were observed. Within the 25th–100th cycles, as depicted in Figure 3d, the elastic modulus exhibited an exponential increase, which correlates with the rapid alignment of

10974628, 0, Downloaded from https://onlinelibrary.wiley.com/doi/10.1002/app.55546 by Florida International University, Wiley Online Library on [19/04/2024]. See the Terms and Conditions (https://onlinelibrary.wiley.com/terms-and-conditions) on Wiley Online Library for rules of use; OA articles are governed by the applicable Creative Commons License

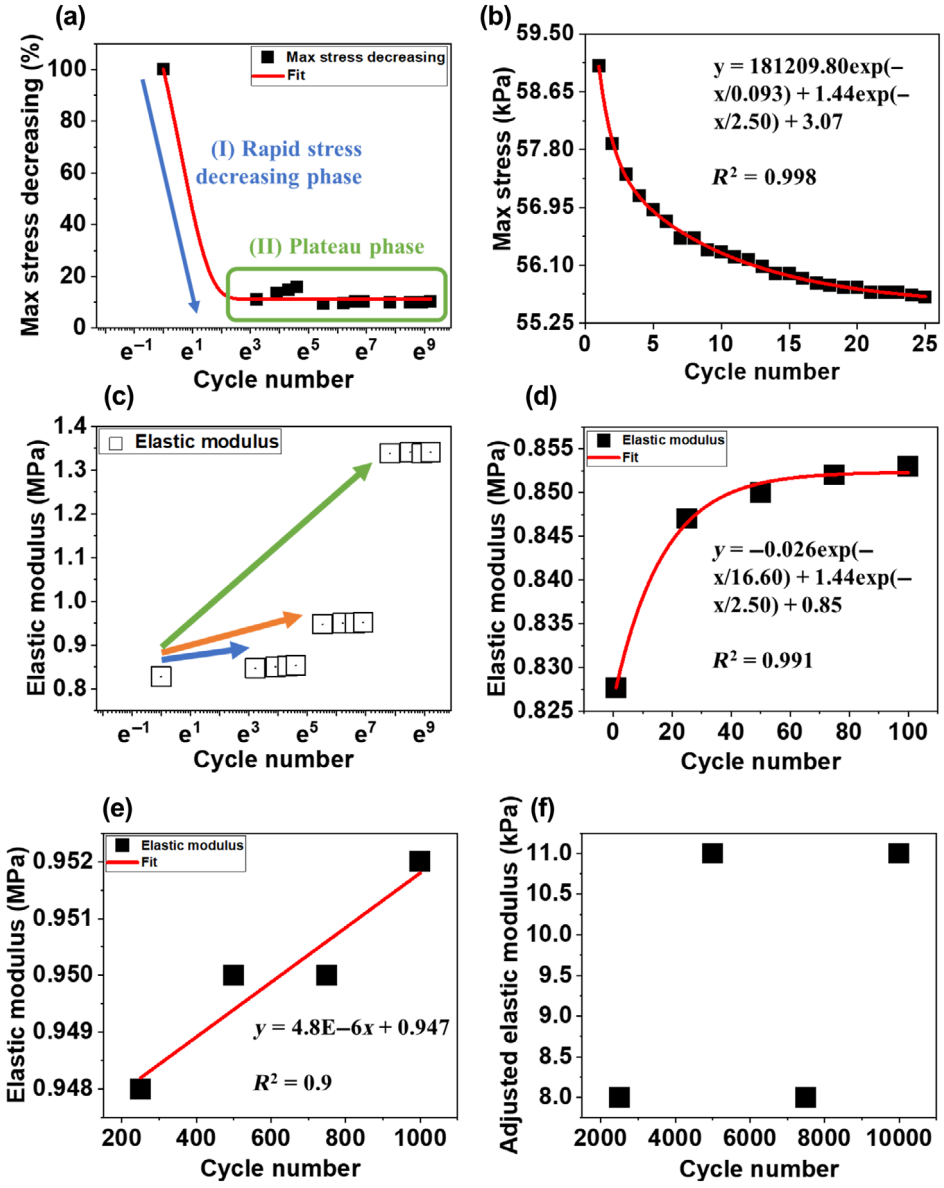

FIGURE 3 Stress softening and strain hardening ($n = 3$). (a) Quantitative reduction in maximum stress, expressed as a percentage, observed at specific intervals (25th, 50th, 75th, 100th, 250th, 500th, 750th, 1000th, 2500th, 5000th, 7500th, and 10,000th cycles) compared to the initial cycle. (b) Maximum stress and cycle relationship of the initial 25 cycles. (c) Elastic modulus at 25th, 50th, 75th, 100th, 250th, 500th, 750th, 1000th, 2500th, 5000th, 7500th, and 10,000th testing cycles. (d) Elastic modulus and cycle relationship of the initial 100 tensile testing cycles. (e) Study of the elastic modulus–cycle relationship within the 250–1000 cycle range. (f) Investigation of the elastic modulus–cycle relationship of 2500–10,000 cycles. [Color figure can be viewed at wileyonlinelibrary.com]

polymer chains. For the subsequent cycles ranging from the 250th to 1000th, the increase in elastic modulus followed a linear trend in Figure 3e. In the later stage of 2500th–10,000th cycles, the elastic modulus showed slight increments without a discernible pattern, as shown in Figure 3f. These observations suggest an increased in PDMS stiffness, attributable of strain-induced crystallization. The stiffness increase is due to the formation of more ordered molecular structures and the alignment of polymer chains under cyclic loading, thereby confirming the occurrence of strain hardening.[16]

3.2 | Cyclic indentation testing of PDMS μ-pillar

In practical applications, the stiffness (or spring constant) of the PDMS μ-pillar is used to calculate contractility behaviors of beating cardiac cells/tissues. For example, Pandey et al.[25] employed the displacement of PDMS μ-pillar as a metric to measure the beating and adhesive forces of cardiomyocytes. Beyond the single-cell level, advanced PDMS-based platforms have been extensively adopted to evaluate the contractile behaviors of engineered cardiac microbundles.[13,14,21,22] Nevertheless, the stress relaxation and strain hardening observed in the tensile testing of bulk PDMS samples raise concerns about the reliability of employing a single stiffness measurement of PDMS μ-pillars for predicting the contractile forces in cardiomyocytes and cardiac tissues. Therefore, we conducted cyclic indentation tests on PDMS μ-pillars. Figure 4a illustrates the load–displacement curves of 5-cycle, including two distinct phases: the deflection (or loading) and recovery (or unloading) phases. A video of this repetitive indentation process is available in Video S1. The corresponding load–displacement and

10974628, 0, Downloaded from https://onlinelibrary.wiley.com/doi/10.1002/app.55546 by Florida International University, Wiley Online Library on [19/04/2024]. See the Terms and Conditions (https://onlinelibrary.wiley.com/terms-and-conditions) on Wiley Online Library for rules of use; OA articles are governed by the applicable Creative Commons License

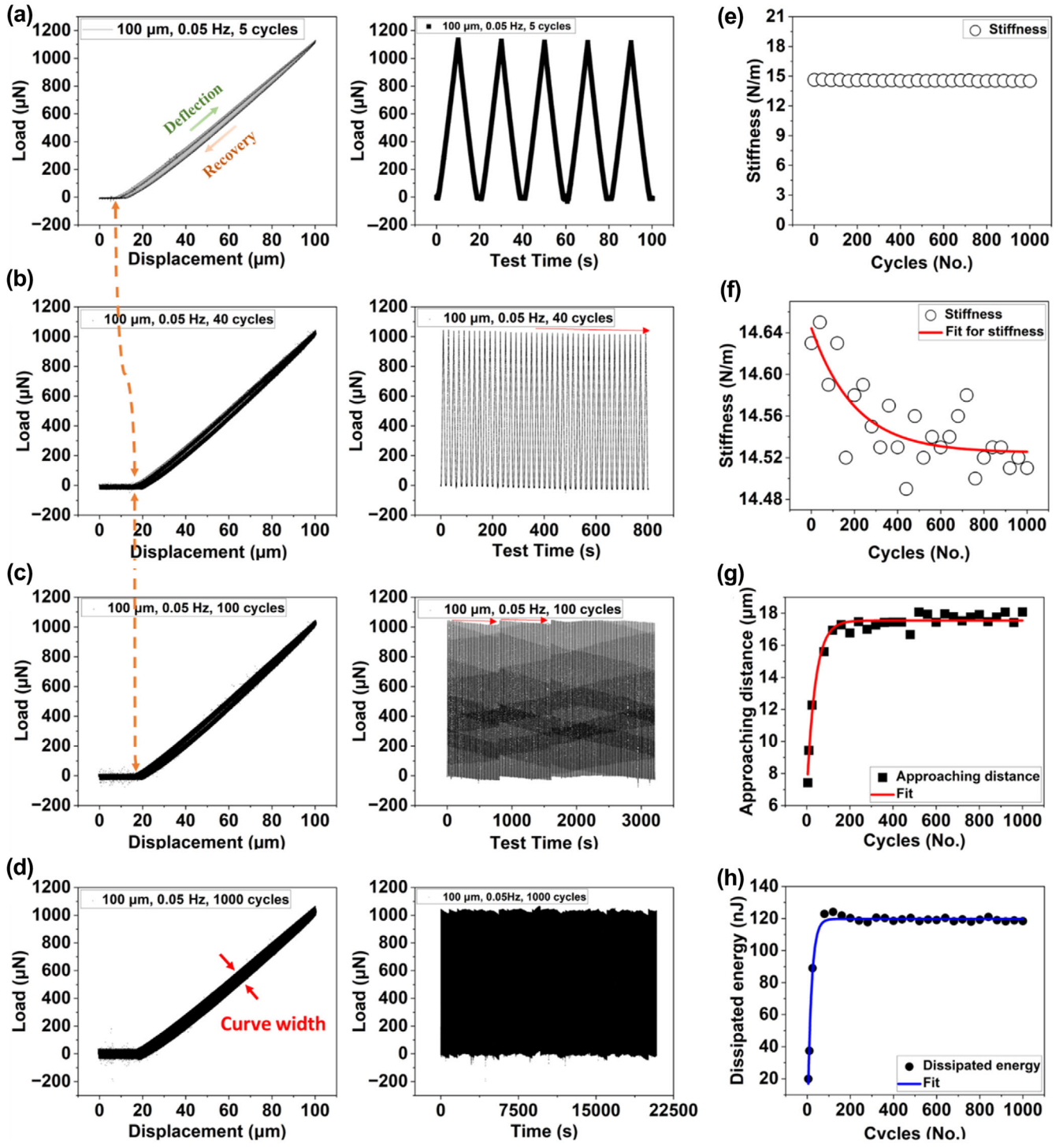

FIGURE 4 Cyclic indentation test of PDMS μ-pillar. (a–d) Load–displacement and load–time curves of 5, 40, 100, and 1000 nanoindentation cycles, respectively. (e,f) Relationship between the tested PDMS μ-pillar stiffness and the number of indentation cycles. (g) Relationship between the approaching distance and the number of indentation cycles. (h) Relationship between the dissipated energy and the number of indentation cycles. PDMS, polydimethylsiloxane. [Color figure can be viewed at wileyonlinelibrary.com]

load-time curves for 40, 100, and 1000 indentation cycles were represented in Figure 4b–d, respectively. Upon applying a maximum displacement of 100 μm (equivalent to ~ 25% of the μ-pillar's diameter), the observed peak load ranged between 1000 and 1200 μN range. Despite minor fluctuations (indicated by red arrows) in the maximum load, the load-time and load–displacement curves maintained a nearly identical morphological pattern for

10974628, 0, Downloaded from https://onlinelibrary.wiley.com/doi/10.1002/app.55546 by Florida International University, Wiley Online Library on [19/04/2024]. See the Terms and Conditions (https://onlinelibrary.wiley.com/terms-and-conditions) on Wiley Online Library for rules of use; OA articles are governed by the applicable Creative Commons License

the initial 100 cycles. Notably, with repetitive indentation extending to 1000 cycles, a visualizable increase in the load–displacement curve width was note, suggesting load fluctuations. To assess the impact of load fluctuation on μ-pillar mechanical property across cycles, stiffness values corresponding to the initial cycle and at specific 40 n cycles (where $1 \leq n \leq 25$, and n denotes a positive integer) are calculated and presented in Figure 4e,f. The stiffness of the μ-pillar, ~15 N/m, remains consistent across 1000 cycles, as depicted in Figure 4e. Upon closer analysis, as illustrated in Figure 4f, the data indicates a 0.82% reduction in stiffness from 14.64 to 14.52 N/m, reaching stabilization ~600th cycle. The stability of stiffness suggests the robustness of PDMS devices to predict the contractile forces in cardiomyocytes and cardiac tissues. Meanwhile, the observed stiffness reduction phenomena can be attributed to stress relaxation, which occurs due to the reorientation of molecular chains in alignment with the direction of the applied external force. This is manifesting as minor fluctuations in the load, as shown in Figure 4b–d.

Referring back to the load–displacement curves presented in Figure 4a–d, two other prominent characteristics can be observed: (1) the approaching distance (marked by the yellow arrows) and (2) the energy dissipation. The approaching distance refers to the displacement extent at a load of 0 N. As depicted in Figure 4g, there was a notable increase in the approaching distance from 7.43 to 16.94 μm over the initial 120 cycles, subsequently reaching a plateau. This observed incomplete recovery indicates creep characteristics of PDMS μ-pillar, attributing to an initial viscous response similar to that observed in bulk tensile testing. The approaching distance and indentation cycle relationship adheres to an exponential growth pattern, characterized by a fitting equation and R^2 of $y = -10.89\exp\left(-\frac{x}{39.50}\right) + 17.55$ and 0.975, respectively. The calculated growth constant of 0.025, is more than 400-fold lower than the rapid decay constant derived from the observed reduction in maximum stress for PDMS tensile testing. This disparity suggests a slower process of chain alignment or the disentanglement of molecular entanglements for PDMS μ-pillar cyclic indentation. This phenomenon is potentially attributed to the orientation of the device's length direction being perpendicular, rather than parallel, to the direction in which the load is applied.

The dissipated energy corresponds to the area enclosed by the load–displacement curves,[24] shown as the gray region in Figure 4a. The relationship between dissipated energy and the indentation cycle is illustrated in Figure 4h. As displayed, the dissipated energy experienced a rapid fourfold increase during the initial 80 cycles, followed by a plateau. Similar to the trend observed in the approaching distance, the dissipated energy also follows an exponential growth pattern. This behavior is characterized by a fitting equation of $y = -136.78\exp(-x/17.52) + 3.07$ with an associated R^2 value of 0.992. The differences in plateau locations among stiffness, approaching distance, and dissipated energy suggest the presence of lagging hysteresis effects. The initial plateauing of the dissipated energy can be attributed to the rapid absorption and release of energy, a consequence of internal friction and the rearrangement of polymer chains. Subsequently, these alterations induce creep behavior and viscoelastic recovery, culminating in the plateauing of the approaching distance. Finally, these aforementioned changes facilitate molecular reorientation and stabilization, ultimately resulting in a delayed equilibrium in the material's stiffness.

3.3 | Mechanisms of time-dependent deformation at meso- and micro-level

For PDMS meso-level tensile testing, it is evident that they are susceptible to stress relaxation and strain hardening[26] when subjected to cyclic stretching ≤20%, primarily stemming from the dynamics of the macromolecular polymer chains: movement, interactions, and subsequent reorganization.[27] Figure 5a elucidates the entanglement of macromolecular chains along the gauge length of a tensile sample, postulating an idealized scenario wherein all chains, uniform in size, exhibit

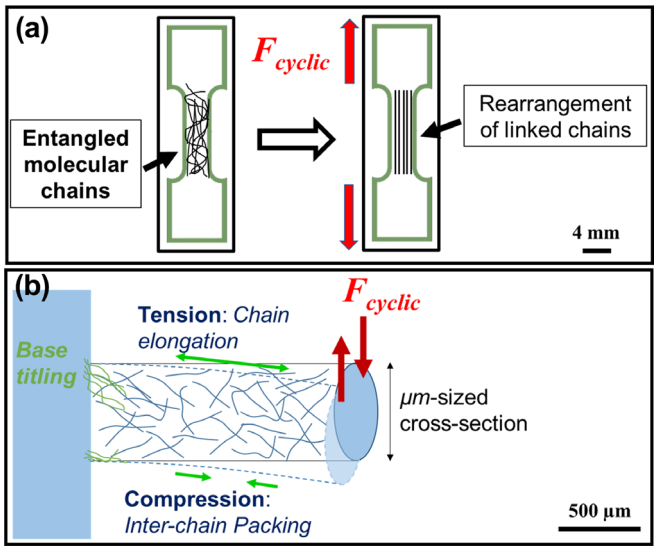

FIGURE 5 PDMS deformation mechanisms at bulk and micro-level. (a) Bulk PDMS tensile samples under uniaxial external stretching force. (b) PDMS μ-pillar under uniaxial external compression force. PDMS, polydimethylsiloxane. [Color figure can be viewed at wileyonlinelibrary.com]

10974628, 0, Downloaded from https://onlinelibrary.wiley.com/doi/10.1002/app.55546 by Florida International University, Wiley Online Library on [19/04/2024]. See the Terms and Conditions (https://onlinelibrary.wiley.com/terms-and-conditions) on Wiley Online Library for rules of use; OA articles are governed by the applicable Creative Commons License

unrestricted mobility and are oriented parallel to the stretching direction. In reality, those chains with PDMS matrix exhibit high extensibility undergo a progressive straightening and sliding process,[27–29] manifesting as elastic deformation. The SEM images in Figure 6a,b illustrate a 5–10-fold decrease in the diameter of microfibrillar structures within the PDMS, observed along the axis of cyclic loading before and after the application of 10,000 cycles. This serves as experimental validation for the mechanisms described above. From a theoretical standpoint, the source of elastic free energy in a polymer matrix is the internal energy borne out of interactions between polymer chains.[28] Concurrently, less flexible chains experience a slow dissociation, which amplifies energy dissipation.[27] Both phenomena operate in tandem until the rearranged macromolecular network stabilizes at mechanical equilibrium.[27]

Compared to tensile testing, cyclic indentation on μ-pillar reveals lagging hysteresis effects and slightly changes in stiffness across 1000 cycles. As depicted in Figure 5b, polymer chains at the uppermost surface layer of μ-pillar, where the force is applied, experience tension.

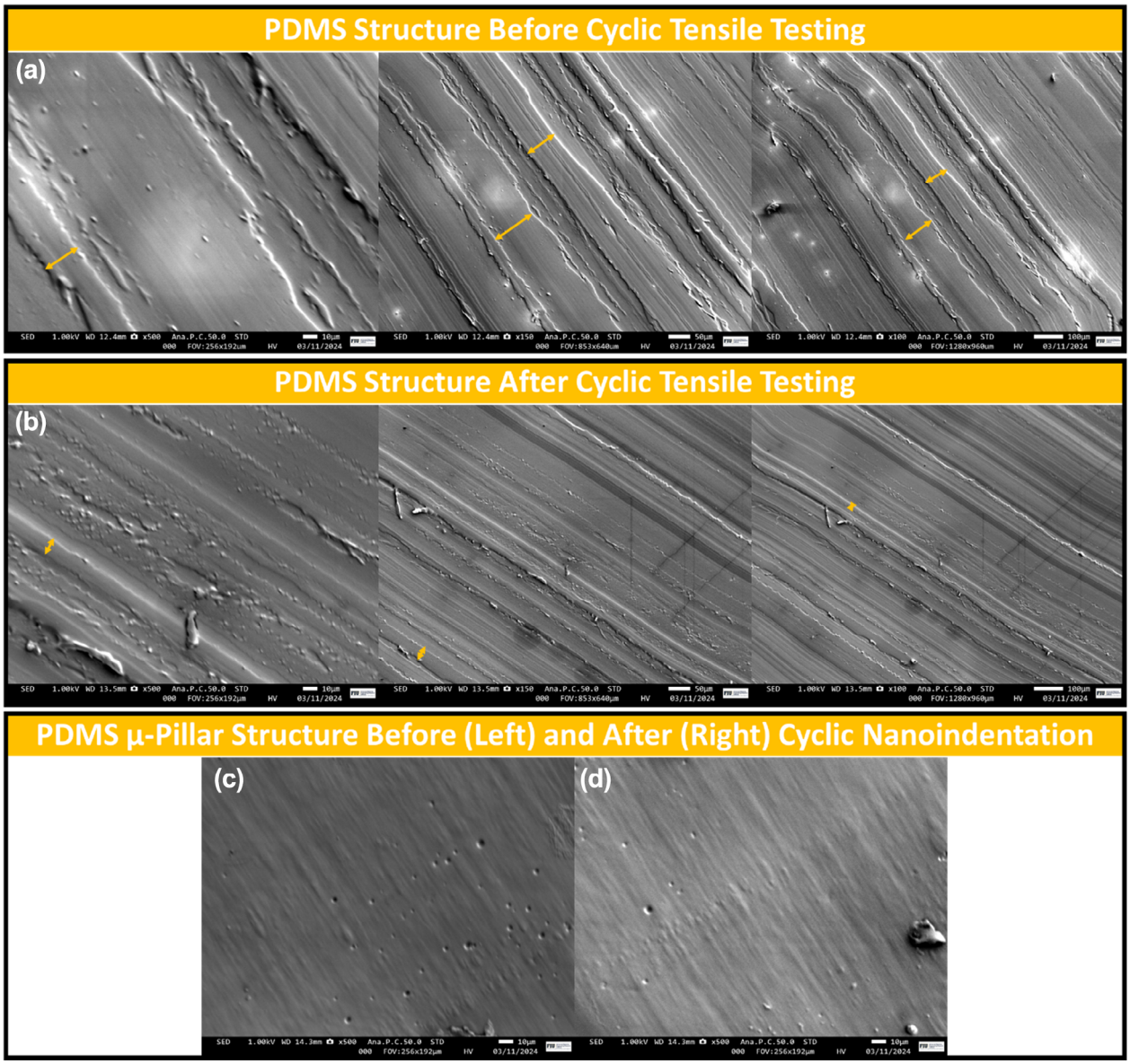

FIGURE 6 Structural morphology of PDMS tensile specimens and μ-pillars, observed pre- and post-cyclic loading. (a,b) SEM images at magnifications of 500×, 150×, and 50× show the structures of dog-bone tensile specimens before and after subjecting 10,000 loading cycles, respectively. (c,d) SEM images at a 500× magnification, presenting the structures of μ-pillars prior to and following 1000 cycles of cyclic nanoindentation testing, respectively. PDMS, polydimethylsiloxane; SEM, scanning electron microscope. [Color figure can be viewed at wileyonlinelibrary.com]

10974628, 0, Downloaded from https://onlinelibrary.wiley.com/doi/10.1002/app.55546 by Florida International University, Wiley Online Library on [19/04/2024]. See the Terms and Conditions (https://onlinelibrary.wiley.com/terms-and-conditions) on Wiley Online Library for rules of use; OA articles are governed by the applicable Creative Commons License

This induces a cyclical process where macromolecular chains are straightened and subsequently recover.[30] In this context, chain disentanglement phenomena and rapid alignment[31] are more restrained compared to tensile testing. This is primarily because the direction of the applied force does not coincide with μ-pillar length. Hence, the chains recuperate gradually with relatively lower internal frictions and energy dissipation compared to tensile testing. A portion of this dissipation arises from the release of energy embedded[31] within the biomaterials during the fabrication process of the μ-pillar. Concurrently, a fraction of the energy is transferred to the junction or foundational region between the μ-pillar and the overarching PDMS base, culminating in a slight tilting of the base. Schoen et al.,[32] have quantified this base tilt to constitute approximately 10%–30% of the total deflection, which is a consequence of the casting process. This engenders an interconnection between the μ-pillar and its base, thereby diminishing forces distributed along the μ-pillar's expanse. The morphological analysis of μ-pillars, before and after subjecting them to 1000 cycles of nanoindentation as depicted in Figure 6c,d, reveals no substantial structural differences. This indirectly supports the hypothesis described above. In parallel, the macromolecular chains at the bottom surface layer (antipodal to where the force is applied) are subjected to a compressive force, thereby fostering instantaneous repacking of inter-chains. Accumulatively, the recovery process induces increasing in approaching distance and reduction of stiffness with the lagging hysteresis effects.

4 | CONCLUSIONS

In this research, we investigated the cyclic mechanical properties of bulk PDMS tensile samples and μ-pillars under conditions of large cycle and low strain, employing tensile and nanoindentation techniques. The tensile testing results revealed a rapid reduction of 90% in dissipated energy after the initial 25 cycles. This is attributed to decreased internal friction and the synergistic effects of stress relaxation and strain hardening. The stress relaxation was evidenced by a rapid dual-phase exponential decay in maximum stress. The first phase constant of 10.75 signifies rapid chain alignment or entanglement disentangling, while the second phase constant of 0.4 indicates long-term structural rearrangement. Contrasting with the behavior of maximum stress, the elastic modulus showed incremental increases of ∼2.75%, 14.78%, and 61.84% at cycle intervals of 25–100th, 250–1000th, and 2500–10,000th, respectively, relative to the modulus at the first cycle. This suggests an increase in PDMS stiffness, potentially due to strain-induced crystallization. Compared to bulk tensile testing, μ-pillars exhibited a lagging hysteresis effect. The early plateauing of dissipated energy is potentially due to rapid energy absorption and release, resulting from internal friction and polymer chain rearrangement. These changes lead to creep behavior and viscoelastic recovery, which is followed by the plateauing of the approaching distance. Ultimately, these modifications aid in molecular reorientation and stabilization, culminating in a delayed equilibrium in the material's stiffness. In this setting, phenomena such as chain disentanglement and rapid alignment are more constrained compared to tensile testing. This is primarily due to the misalignment between the direction of the applied force and the length of the μ-pillars. Therefore, the chains recover more gradually, with relatively lower internal frictions and energy dissipation compared to those observed in tensile testing.

AUTHOR CONTRIBUTIONS

Lihua Lou: Data curation (lead); formal analysis (lead); funding acquisition (equal); investigation (lead); methodology (lead); project administration (lead); supervision (lead); validation (lead); visualization (lead); writing – original draft (lead); writing – review and editing (lead). **Nicole Bacca:** Data curation (equal); formal analysis (equal); methodology (equal). **Marshall S. Ma:** Methodology (supporting). **Pranjal Nautiyal:** Conceptualization (supporting); methodology (supporting); visualization (equal). **Thomas G. Bifano:** Methodology (supporting). **Arvind Agarwal:** Conceptualization (equal); funding acquisition (lead); project administration (equal); resources (lead); supervision (equal).

ACKNOWLEDGMENTS

This work was supported by the CELL-MET Engineering Research Centers Program of the National Science Foundation under NSF Cooperative Agreement No. EEC-1647837. L.L. is grateful for the funding provided by the Florida Heart Foundation.

CONFLICT OF INTEREST STATEMENT

The authors declare no conflicts of interest.

DATA AVAILABILITY STATEMENT

The data that support the findings of this study are available from the corresponding author upon reasonable request.

ORCID

Lihua Lou https://orcid.org/0000-0001-5283-6211

REFERENCES

[1] T. K. Kim, J. K. Kim, O. C. Jeong, *Microelectron. Eng.* **1982**, *2011*, 88.

[2] D. Qi, K. Zhang, G. Tian, B. Jiang, Y. Huang, *Adv. Mater.* **2021**, *33*, 2003155.

10974628, 0, Downloaded from https://onlinelibrary.wiley.com/doi/10.1002/app.55546 by Florida International University, Wiley Online Library on [19/04/2024]. See the Terms and Conditions (https://onlinelibrary.wiley.com/terms-and-conditions) on Wiley Online Library for rules of use; OA articles are governed by the applicable Creative Commons License

[3] F. Schneider, T. Fellner, J. Wilde, U. Wallrabe, *J. Micromech. Microeng.* **2008**, *18*, 065008.
[4] J.-H. Seo, K. Sakai, N. Yui, *Acta Biomater.* **2013**, *9*, 5493.
[5] I. Miranda, A. Souza, P. Sousa, J. Ribeiro, E. M. Castanheira, R. Lima, G. Minas, *J. Funct. Biomater.* **2021**, *13*, 2.
[6] A. Marsano, C. Conficconi, M. Lemme, P. Occhetta, E. Gaudiello, E. Votta, G. Cerino, A. Redaelli, M. Rasponi, *Lab Chip.* **2016**, *16*, 599.
[7] L. K. Fiddes, N. Raz, S. Srigunapalan, E. Tumarkan, C. A. Simmons, A. R. Wheeler, E. Kumacheva, *Biomaterials* **2010**, *31*, 3459.
[8] Z. Jiang, N. Chen, Z. Yi, J. Zhong, F. Zhang, S. Ji, R. Liao, Y. Wang, H. Li, Z. Liu, *Nat. Electron.* **2022**, *5*, 784.
[9] R. Zizhou, K. Khoshmanesh, X. Wang, S. Houshyar, *ACS Appl. Mater. Interfaces.* **2023**, *15*, 35411.
[10] G. Mishra, S. Bhattacharyya, V. Bhatia, B. Ateeq, A. Sharma, S. Sivakumar, *ACS Appl. Mater. Interfaces.* **2017**, *9*, 34625.
[11] K. Ronaldson-Bouchard, K. Yeager, D. Teles, T. Chen, S. Ma, L. Song, K. Morikawa, H. M. Wobma, A. Vasciaveo, E. C. Ruiz, *Nat. Protoc.* **2019**, *14*, 2781.
[12] D.-S. Kim, Y. W. Choi, A. Shanmugasundaram, Y.-J. Jeong, J. Park, N.-E. Oyunbaatar, E.-S. Kim, M. Choi, D.-W. Lee, *Nat. Commun.* **2020**, *11*, 535.
[13] L. Lou, A. S. Rubfiaro, J. He, A. Agarwal, *Adv. Mater. Technol.* **2021**, *6*, 2100669.
[14] A. Sesena-Rubfiaro, N. J. Prajapati, L. Paolino, L. Lou, D. Cotayo, P. Pandey, M. Shaver, J. D. Hutcheson, A. Agarwal, J. He, *ACS Biomater. Sci. Eng.* **2023**, *9*, 1644.
[15] Z. Wang, A. A. Volinsky, N. D. Gallant, *J. Appl. Polym. Sci.* **2014**, *131*, 41050.
[16] W. Lee, K. Yeo, A. Andriyana, Y. Shee, F. M. Adikan, *Mater. Des.* **2016**, *96*, 470.
[17] A. R. Babu, N. Gundiah, *Mater. Res. Express.* **2018**, *5*, 085310.
[18] K. Song, N.-K. Cho, K. Park, C.-S. Kim, *Polymer* **2022**, *14*, 2373.
[19] J. Javor, S. Sundaram, C. S. Chen, D. J. Bishop, *J. Microelectromech. Syst.* **2020**, *30*, 96.
[20] L. Lou, J. Wang, S. Ramkumar, *J. Appl. Polym. Sci.* **2019**, *136*, 47159.
[21] M. S. Ma, S. Sundaram, L. Lou, A. Agarwal, C. S. Chen, T. G. Bifano, *Front. Bioeng. Biotechnol.* **2023**, *11*, 703.
[22] H. Li, S. Sundaram, R. Hu, L. Lou, F. Sanchez, W. McDonald, A. Agarwal, C. S. Chen, T. G. Bifano, *IEEE Trans. Biomed. Eng.* **2023**, *70*, 2237.
[23] Y.-M. Lin, L. Paolino, L. Lou, A. Herrera, E. Pierre, A. Agarwal, S. Ramaswamy, *J. Biomech.* **2022**, *138*, 111129.
[24] L. Lou, A. S. Rubfiaro, J. He, A. Agarwal, *Nanoscale* **2023**, *15*, 10360.
[25] P. Pandey, W. Hawkes, J. Hu, W. V. Megone, J. Gautrot, N. Anilkumar, M. Zhang, L. Hirvonen, S. Cox, E. Ehler, *Dev. Cell.* **2018**, *44*, 326.
[26] T. Barriere, X. Gabrion, S. Holopainen, J. Jokinen, *Int. J. Plast.* **2020**, *135*, 102781.
[27] V. Morovati, A. Bahrololoumi, R. Dargazany, *Int. J. Plast.* **2021**, *142*, 102993.
[28] F. Tanaka, S. Edwards, *Macromolecules* **1992**, *25*, 1516.
[29] E. Delebecq, N. Hermeline, A. Flers, F. Ganachaud, *ACS Appl. Mater. Interfaces.* **2012**, *4*, 3353.
[30] M. Heras Segura, K. V. Singh, F. Khan, *ASME International Mechanical Engineering Congress and Exposition.* **2019**, *4*, V004T05A053.
[31] F. Carleo, J. Plagge, R. Whear, J. Busfield, M. Klüppel, *Polymer* **2020**, *12*, 841.
[32] I. Schoen, W. Hu, E. Klotzsch, V. Vogel, *Nano Lett.* **2010**, *10*, 1823.

SUPPORTING INFORMATION

Additional supporting information can be found online in the Supporting Information section at the end of this article.

How to cite this article: L. Lou, N. Bacca, M. S. Ma, P. Nautiyal, T. G. Bifano, A. Agarwal, *J. Appl. Polym. Sci.* **2024**, e55546. https://doi.org/10.1002/app.55546

10974628, 0, Downloaded from https://onlinelibrary.wiley.com/doi/10.1002/app.55546 by Florida International University, Wiley Online Library on [19/04/2024]. See the Terms and Conditions (https://onlinelibrary.wiley.com/terms-and-conditions) on Wiley Online Library for rules of use; OA articles are governed by the applicable Creative Commons License